ARTICLES
PUBLISHED ONLINE: 12 JANUARY 2015 | DOI: 10.1038/NCHEM.2142
nature chemistry

Rational design of functional and tunable oscillating enzymatic networks

Sergey N. Semenov[1†], Albert S. Y. Wong[1†], R. Martijn van der Made[1], Sjoerd G. J. Postma[1], Joost Groen[1], Hendrik W. H. van Roekel[2], Tom F. A. de Greef[2] and Wilhelm T. S. Huck[1*]

Life is sustained by complex systems operating far from equilibrium and consisting of a multitude of enzymatic reaction networks. The operating principles of biology's regulatory networks are known, but the *in vitro* assembly of out-of-equilibrium enzymatic reaction networks has proved challenging, limiting the development of synthetic systems showing autonomous behaviour. Here, we present a strategy for the rational design of programmable functional reaction networks that exhibit dynamic behaviour. We demonstrate that a network built around autoactivation and delayed negative feedback of the enzyme trypsin is capable of producing sustained oscillating concentrations of active trypsin for over 65 h. Other functions, such as amplification, analog-to-digital conversion and periodic control over equilibrium systems, are obtained by linking multiple network modules in microfluidic flow reactors. The methodology developed here provides a general framework to construct dissipative, tunable and robust (bio)chemical reaction networks.

The response of living cells to physicochemical changes in their environment is regulated by complex integrated networks of reactions that control the functioning of biomolecules in space and time. Time-keeping, chemical amplification and signal modulation are examples of essential functions in signal transduction, vision, metabolic regulation and cell division in biological systems[1,2]. These functions are 'encoded' in complex networks of biochemical reactions that operate far from equilibrium[3,4]. In contrast, the dynamics of responsive synthetic materials are governed by reversible processes and are therefore limited by the relaxation towards chemical equilibrium[5–7]. Chemical reaction networks (CRNs) arise out of the myriad interactions between the components of the cell, and their characteristics transcend the properties of individual molecules and reactions. In recent years it has become possible to design synthetic gene networks to control some of the fundamental properties of living systems[8,9], but to create synthetic dynamic molecular systems that capture the extraordinary richness in behaviour displayed by living cells remains a major challenge. Significant efforts have been made in applying the principal regulatory motifs of biochemical reaction networks to dissipative systems based on DNA replication and transcription[10–14]. Complex spatio-temporal pattern formation has been observed in the classic example of Belousov–Zhabotinsky (BZ) oscillations[15] and, together with related CRNs, these have been harnessed into a rich variety of self-organizing systems[16–19]. Now, we wish to exploit the full power of chemical synthesis to construct CRNs tuned by small molecules approaching the tunability and functionality of living systems. Although impressive progress in this direction has been made[20–25], we lack a general methodology based on rational design that integrates the structure of (small) molecules with the tuning of the reaction rates for each step in the network. We require a modular approach using common building blocks and reaction conditions, and the ability to program a functional output of the network. Oscillations are a well-established hallmark of out-of-equilibrium CRNs and, inspired by metabolic networks[26,27], we present a methodology for constructing tunable, oscillating reaction networks based on enzymatic conversions of small molecules. Importantly, the output of these CRNs is a periodically changing concentration of a catalyst, and, by coupling multiple reactors, this chemical signal can be modulated and processed further[28].

Results

Choosing network topology and key components. Theoretical analyses have revealed numerous regulatory motifs in biochemical networks that give stable oscillations[27,29,30]. The design of our CRN is based on a time-delayed negative feedback topology, combined with a short positive feedback loop (Fig. 1a). To reduce our design to practice, we selected enzymes whose activities can be modulated by small molecules. Trypsin (*Tr*) is the key element in our CRN, and positive feedback arises from the autocatalytic conversion of the enzymatically inactive trypsinogen (*Tg*) into *Tr*[31]. To create the negative feedback loop, an active inhibitor must be formed as a result of the enzymatic activity of *Tr*. There are various known inhibitors for *Tr*, and here we use the strong and irreversible inhibitor 4-[2-aminoethyl]benzenesulfonyl fluoride (Inh, Fig. 1b) as the key small molecule in our CRN as it can be modified easily. It is essential that the negative feedback resulting in *Tr* inhibition is delayed with respect to *Tr* production. We therefore split the negative feedback loop into two orthogonal steps, each amenable to rate-tuning. First, *Tr* cleaves the Lys residue of the proinhibitor, the N-terminus of which was acetylated to yield a well-soluble molecule and an endopeptidase substrate. Second, aminopeptidase M (*Ap*) cleaves an amino acid residue from the intermediate inhibitor, thereby activating the inhibitor.

Finding conditions for sustained oscillations. Before we assembled the network, individual, isolated reactions or small parts of the network were studied using kinetic assays. A number of derivatives of the intermediate inhibitor with different amino acids conjugated to Inh were synthesized, showing different enzymatic conversion rates (Supplementary Sections 2 and 3). The Gln-derivative (H-Gln-Inh) showed the lowest background

[1]Institute for Molecules and Materials, Radboud University Nijmegen, Heyendaalseweg 135, 6525 AJ Nijmegen, The Netherlands. [2]Institute for Complex Molecular Systems, Eindhoven University of Technology, Den Dolech 2, 5600 MB Eindhoven, The Netherlands. †These authors contributed equally to this work. *e-mail: w.huck@science.ru.nl

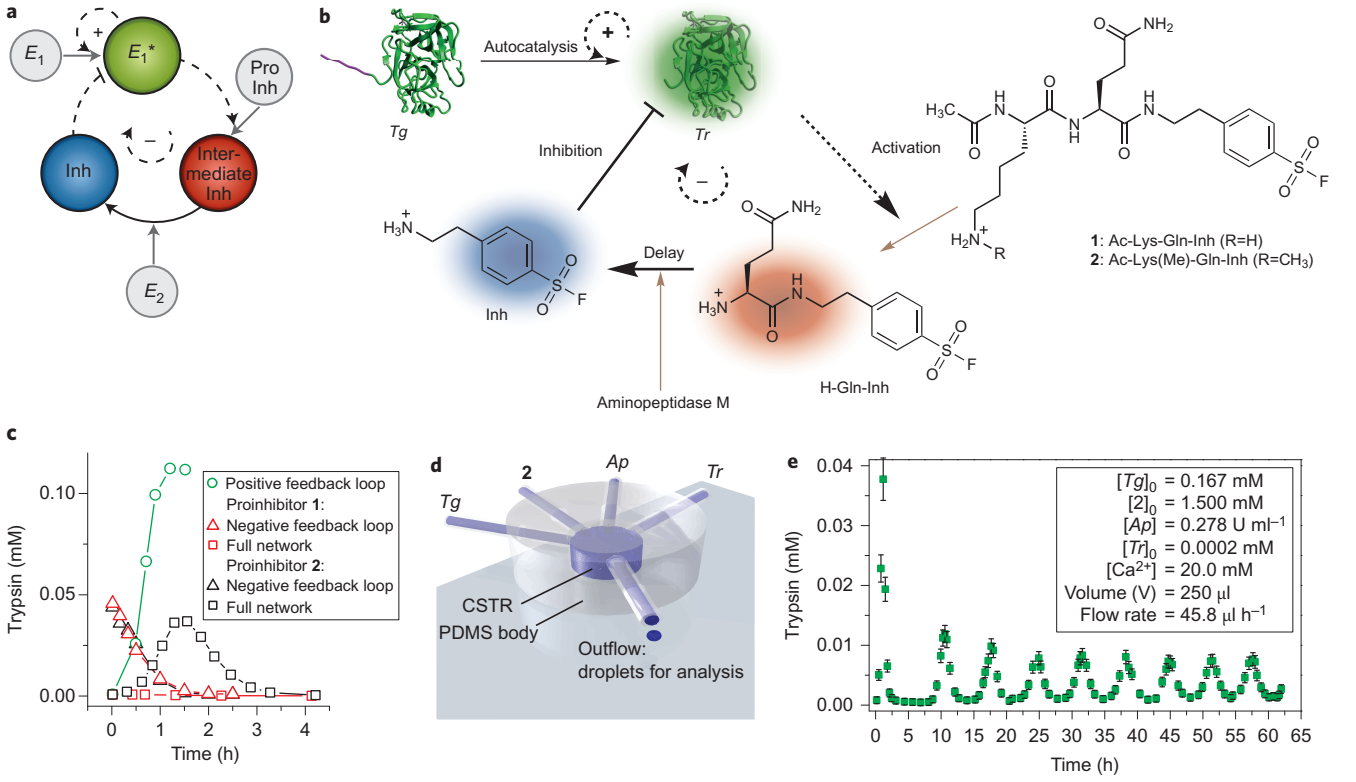

Figure 1 | Rational design and experimental assembly of a flow-based enzymatic oscillator. a, Schematic network layout of the enzymatic oscillator based on autocatalytic production and delayed inhibition of an enzyme. Enzymatically inactive E_1 is converted to active E_1*. In a positive feedback loop, E_1* catalyses its own formation. In addition, E_1* catalyses the first of a two-step sequence that unmasks an inhibitor of itself, with the second step being catalysed by a second enzyme E_2. This two-step process constitutes a negative feedback loop. The combination of positive and negative feedbacks results in an oscillating system. **b**, Detailed reaction diagram of the CRN. **c**, Concentration of *Tr* versus time measured by assembling various parts of the network under batch conditions: autocatalytic production of *Tr* from *Tg* (green), inhibition of *Tr* by Inh produced in the negative feedback loop (red/black triangles) and the complete network (red/black squares). **d**, Schematic representation of the flow reactor. The concentration of *Tr* in the outflow is measured using a standard *Tr* activity assay[31]. **e**, Concentration of *Tr* versus time measured by assembling the complete network under flow conditions at 23 °C. Error bars represent 95% confidence intervals and were calculated from relative experimental errors (Supplementary equations (13)–(15)).

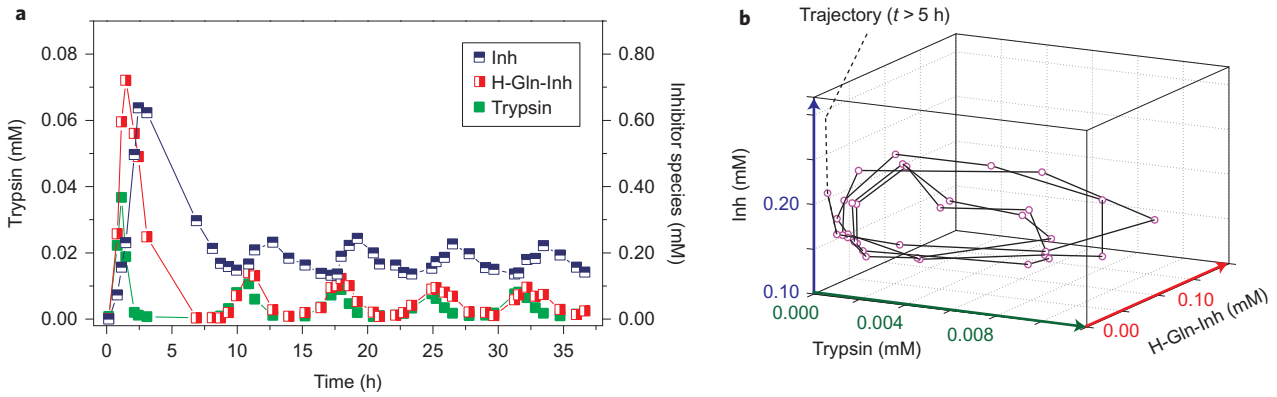

Figure 2 | Characterization of the flow-based enzymatic oscillator. a, Time traces showing the concentration of *Tr*, intermediate inhibitor H-Gln-Inh, and inhibitor in the microfluidic reactor using conditions reported in Fig. 1e. **b**, Phase portrait showing that the dynamics of the flow-based enzymatic oscillator display limit cycle oscillations.

interaction with *Tr* and the fastest activation by *Ap*, giving a good decoupling of the two cleavage steps. After this initial screening, proinhibitor **1** (Ac-Lys-Gln-Inh, Fig. 1b) was used for tests of the CRN in batch. Figure 1c shows how the positive and negative feedback loops function as separate elements: autocatalytic *Tg* activation by *Tr* shows an exponential increase in [*Tr*] (green dots). Conversely, [*Tr*] drops rapidly in the isolated negative feedback loop containing **1** and *Ap* (red triangles). However, when all elements of the network are combined, there is no significant response in the system (red squares) and [*Tr*] remains low, indicating that the negative feedback loop either initiates too quickly or is too fast.

The flexible design now allows us to balance the negative feedback loop by either changing the binding constant between the

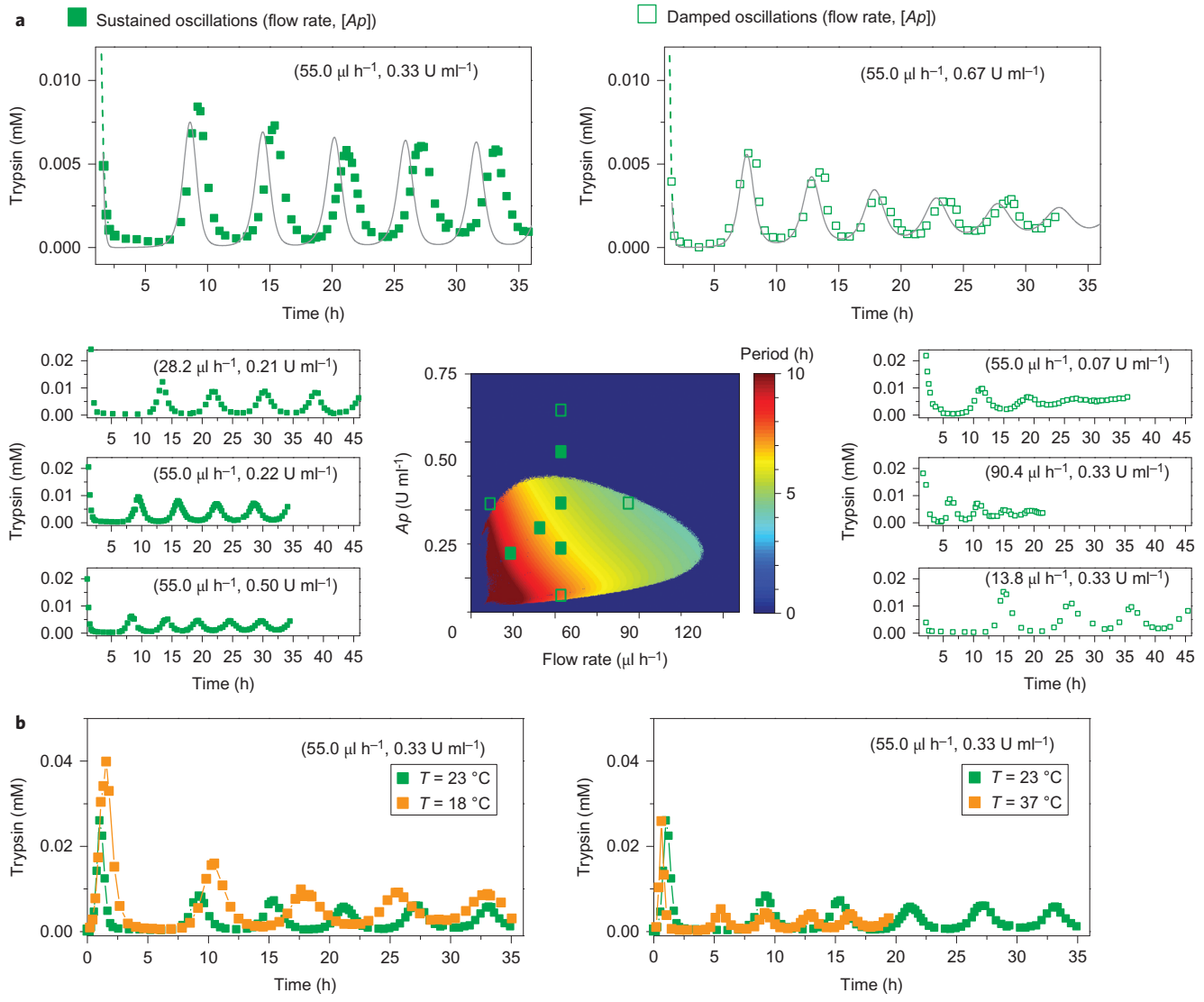

Figure 3 | Tunability and robustness of the enzymatic oscillator. a, Time courses in [*Tr*] corresponding to sustained and damped oscillatory behaviour for various values of the flow rate and [*Ap*] (in brackets). Solid lines represent model predictions using optimized parameters. Sustained and damped responses are mapped onto the (flow rate, [*Ap*]) plane. The computed period of the sustained oscillations obtained using the optimized parameter set is displayed as a heat map. **b**, CSTR experiments carried out at different temperatures (18, 23 and 37 °C), showing the robustness of the enzymatic oscillator.

proinhibitor and *Tr*, thereby lowering the sensitivity of the feedback loop to [*Tr*], or by changing [*Ap*] or the amino acid conjugated to the inhibitor, thereby increasing the delayed inhibition. At this point, it is imperative to combine the design of small molecules with mathematical simulation of the complete network. To this end, a set of ordinary differential equations (ODEs) was constructed that accurately describes the reactions of the CRN using mass-action kinetics (Supplementary Table 2). The kinetic parameters of all known reactions in the CRN, including the background hydrolysis of the fluorosulfonyl moiety of the inhibitor, were measured experimentally (Supplementary Table 1) and used as inputs for the simulation (Supplementary Section 4). We note that the proteolytic degradation of enzymes is another potential side reaction. We verified that digestions of *Tr* and *Ap* by *Tr* as well as autodegradation of *Ap* do not take place (at least not at sufficient rates, that is, several hours) and so do not affect the kinetics of the network under the conditions used in our experiments (Supplementary Section 5.1.2). To guide the design of molecules for which a significant response (Supplementary Fig. S14a) of the CRN will be obtained, the model was used to determine the range in kinetic parameters of the enzymatic reactions in the negative feedback that lead to a single peak in [*Tr*] when the full network is combined under batch conditions. The simulations (Supplementary Fig. 14b) show that the rate of the *Ap*-catalysed step is in a range accessible by choosing a suitable [*Ap*], but the enzymatic efficiency of *Tr* acting on **1** is too high (experimental value of $k_{cat}/K_M > 3{,}300\ mM^{-1}\ h^{-1}$, where k_{cat} is the turnover number and K_m is the Michaelis constant of trypsin, Supplementary Fig. 4), as a single peak only occurs if the enzymatic efficiency of this enzymatic step is significantly reduced ($k_{cat}/K_M < 1{,}500\ mM^{-1}\ h^{-1}$). It is known that methylation of the ε-NH_2 in Lys lowers the affinity between the substrate and *Tr*[32], providing a route to molecularly engineer a decreased sensitivity of the negative feedback loop to *Tr*.

We subsequently studied the response of a CRN based on the modified proinhibitor **2** (Fig. 1b) and, although the difference in the rate of *Tr* (43 µM) inhibition by **1** or **2** (free or methylated Lys) in the presence of *Ap* is small (Fig. 1c), networks composed of **2** do indeed give a single oscillation (Fig. 1c, black squares). Similar simulations (Supplementary Fig. 15) were performed under flow conditions (by taking into account the continuous

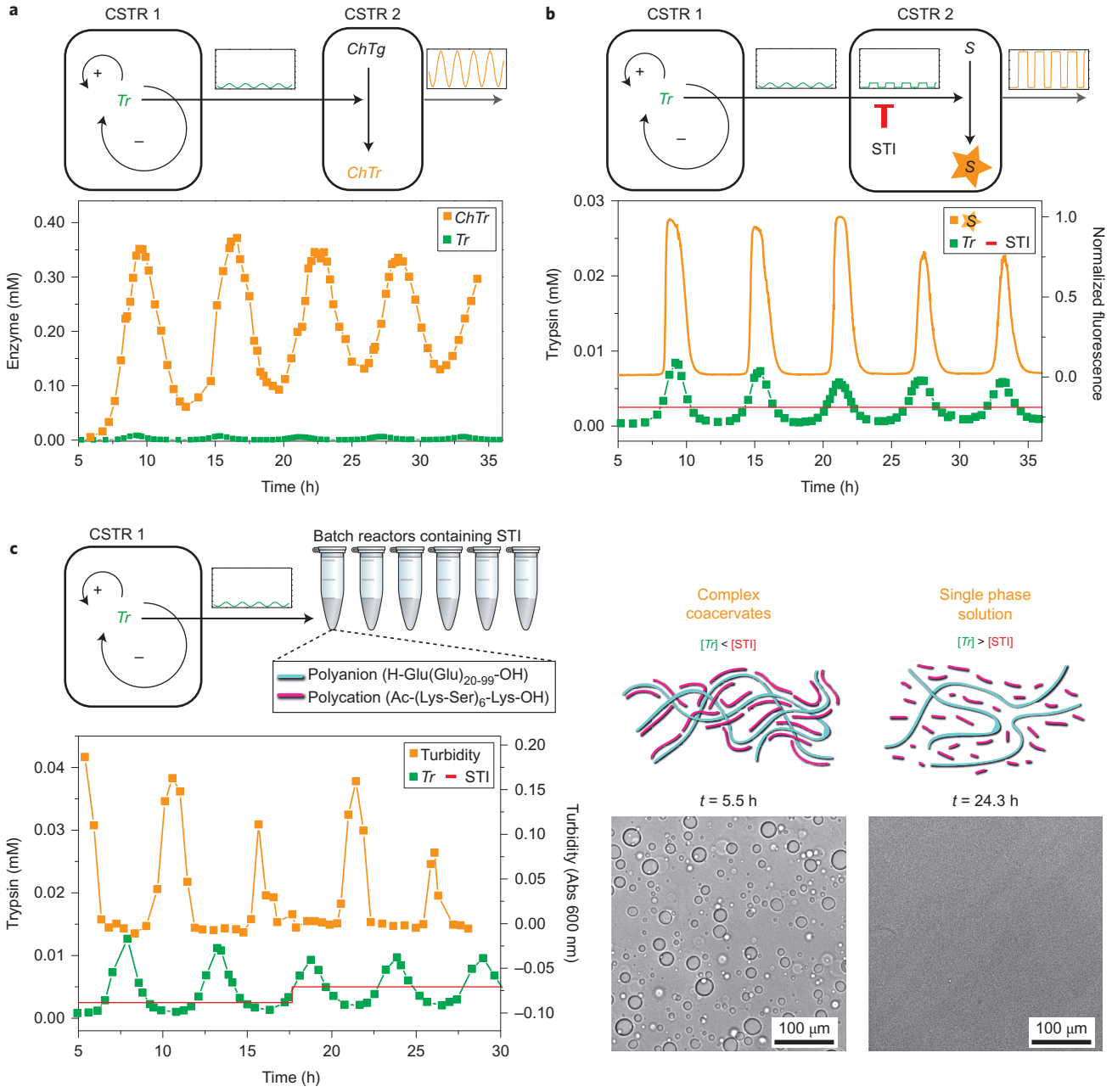

Figure 4 | Coupling of oscillations in trypsin concentration to a variety of chemical and physical processes in systems of two reactors. a, Amplification of oscillations in trypsin concentration by conversion of chymotrypsinogen (*ChTg*) to chymotrypsin (*ChTr*) in coupled CSTRs. An outlet of CSTR 1, analogous to the CSTR in Fig. 1d, is connected to CSTR 2, which has a continuous supply of ChTg. **b**, Conversion of oscillations in trypsin concentration to modulated fluorescent signals. In this case, an outlet of CSTR 1 is connected to CSTR 2, which has a continuous supply of soybean trypsin inhibitor (STI) and a rhodamine-based fluorogenic substrate (S). STI inhibits any trypsin activity below the threshold level (red line, [STI] = 2.5 μM). **c**, Conversion of oscillations in trypsin concentration to the disassembly of complex coacervates formed by polycation (Ac-(Lys-Ser)$_6$-Lys-OH) and polyanion (H-Glu(Glu)$_{20\text{-}99}$-OH). Fractions collected from the outflow of CSTR 1 were mixed in batch reactors containing a solution of polyelectrolytes (1:1 charge ratio) and STI ([STI]$_{0\text{–}18\ h}$ = 2.5 μM, [STI]$_{>18\ h}$ = 5.0 μM). The diagrams show polyglutamic acid (polyanion) in blue and the lysine–serine polycations in pink. Corresponding microscopy images are shown below.

in- and outflow of species in the network, Supplementary Section 4) to support reactions carried out in an open reactor. A fluidic continuously stirred tank reactor (CSTR) was used, with four inlets containing *Tg*, *Ap*, **2** and a catalytic amount of *Tr* (Fig. 1d). We experimentally determined the composition of the reactor by sampling the outflow at regular intervals (14 min), and [*Tr*] was established using a standard *Tr* activity assay (Supplementary Section 5). Guided by simulations, which indicated that [*Ap*] should fall within the range 0.011–0.638 U ml^{-1}, with a flow rate over volume of >0.005 h^{-1}, and in combination with scoping experiments (Supplementary Fig. 25), we determined conditions under which sustained oscillations in [*Tr*] were observed with a period of 6.5 h and an amplitude of 6.6 μM (Fig. 1e).

Properties of the enzymatic oscillator. To determine unambiguously the state of the system, the variation in [Inh] and [H-Gln-Inh] with time were followed using HPLC (Supplementary Section 5). Figure 2a shows that the concentrations of each of these

components of the network oscillate with time. The progress of these variables during the reaction is plotted in the phase portrait in Fig. 2b, which shows a trajectory that initially approaches the steady state of the system but never reaches it. Instead, the system performs self-sustained oscillations corresponding to the development of a periodic orbit surrounding the steady state in the phase portrait. This isolated trajectory is called a limit cycle, and shows that the behaviour is inherent to the nonlinear CRN and is not caused by an external periodic forcing[15].

Biological systems show robustness and tunability[33]. Here, we tested our network for robustness—the persistence of sustained oscillations under external perturbations—by changing global parameters such as the overall flow rate or reaction temperature. Furthermore, varying local or internal parameters such as [*Ap*] or other individual components of the CRN allowed us to tune the period and amplitude of the oscillations. The experiments in Fig. 3a show the behaviour of the system as a function of [*Ap*] and flow rate for experiments carried out at 23 °C. The heat map shows the broad range of concentrations and flow rates for which sustained oscillations are obtained; outside this range the oscillations are damped and the system reaches a steady state. A further exploration of robustness was carried out by probing the temperature dependence of the CRN. Figure 3b shows that the network is capable of performing sustained oscillations at least in the temperature range of 18–37 °C, with periods decreasing from ~7.5 h to ~3.5 h.

Calibrating the model to the data sets for sustained oscillations allowed us to extract kinetic parameters for the complete network (with all reactions interacting). Using a genetic algorithm[34] in which the fitness function is extended by implementing additional constraints, we obtain an optimized set of constants (Supplementary Table 3). The mathematical model with optimized rate constants for the CRN allowed us to compute the phase diagram as shown in Fig. 3a. The computed phase diagram shows the regime in which the sustained oscillations can be found and, although the simulations predict a slightly larger sustained regime, they strongly agree with experimentally observed amplitudes and periods and the overall shape of the phase diagram.

The model also allowed us to expand our analyses by varying other initial concentrations (for example, $[Tg]_0$ and $[\mathbf{2}]_0$) in our system and to probe the influence of the kinetic parameters of individual reactions (inhibition, activation and delay rate constants) on the CRN. Supplementary Fig. 19 presents the parameter value window, amplitude and period of sustained oscillations upon changing selected parameters from 0.1 to 10 times the initial values. For example, the amplitude of sustained oscillations changes by over a factor of 5, and the period nearly halves, when [*Tg*] is changed from 0.78 to 3.44 of the initial [*Tg*], while damped oscillations will be obtained outside this region. Changing the initial [**2**] has very little effect, whereas changing the delay of the feedback loop ($K_{M,delay}$) leads to complex excursions in amplitude and period.

Processing of oscillations by coupling multiple CSTRs. Networks in complex systems are often interlinked, with enzymes playing key roles in multiple processes. To avoid unwanted crosstalk between networks, these are typically separated in space (via compartmentalization in different organelles) or time (by timing the expression of different enzymes). The modular nature of both the network and fluidic reactors offers opportunities to assemble more complex functional networks by linking the output of a first reactor to the inlet of a second reactor. Figure 4a,b show a feedforward design of amplification and thresholding of the signal produced by the first reactor. The oscillator in CSTR 1 produces variations in [*Tr*] within a very narrow band. This 'signal' can be amplified 50-fold when *Tr* is used to activate chymotrypsinogen in the second reactor, and the activity of the chymotrypsin formed is measured. Alternatively, the output can be 'filtered' by introducing 2.5 μM soybean trypsin inhibitor (STI, a strong inhibitor for *Tr*), in the second reactor, which buffers all *Tr* activity below this value. Above the threshold concentration, *Tr* can convert a substrate into a fluorescent product, converting the initial oscillation into a switch-like output.

Finally, we show how an out-of-equilibrium enzymatic network can be coupled to an equilibrium process, by studying the assembly and disassembly of complex coacervates formed between oppositely charged polyelectrolytes[35]. We formed coacervates from polyglutamic acid and a lysine–serine polycation (Supplementary Section 5) that can be cleaved by *Tr*. Degradation of the polycation with increasing [*Tr*] triggers disassembly, and this process can be followed both by measuring the turbidity of the solution and by microscopy (Fig. 4c). The addition of small amounts of STI again leads to switch-like assembly and disassembly of coacervates, depending on the phase of the oscillating CRN.

Discussion

Our studies not only show the complex responsiveness of an enzymatic reaction network showing sustained oscillations, but also provide a new, modular retrosynthetic approach to translate a complex network topology into positive and negative feedback loops with rates tailored by the chemical structures of small molecules. This approach yields detailed criteria for the chemical structure and corresponding reaction rates of each of the components of the network and can be used to program a specific, functional output. The CRNs obtained are robust and maintain sustained oscillations within a certain range of global parameters such as temperature and flow rate. Furthermore, the amplitude and period of the oscillator can be tuned over a relatively broad range and this signal can be further processed by coupling multiple reactor modules, each with a specific enzymatic reaction network.

We anticipate that a suite of more complex network topologies (for example, allowing for homeostasis, adaptation or biosynthetic pathways) can now be designed and synthesized, ultimately creating a broad repertoire of functional CRNs sharing common motifs. The production of an oscillatory concentration of an active enzyme holds considerable potential for coupling to stimuli-responsive gels and other smart materials, which opens up applications in tissue engineering and soft robotics[23]. Our work forms the basis of a bottom-up synthetic biology approach to the development of complex synthetic systems that operate according to the principles of life.

Methods

Full details of the synthesis and characterization of all compounds, screening of (intermediate) proinhibitors to optimize the CRN, kinetic studies, computational simulations and CSTR experiments are provided in the Supplementary Sections 1–5.

Batch experiments. Either proinhibitor **1** or **2** (258 μM) was mixed with trypsinogen (129 μM), trypsin (43 μM) and aminopeptidase (0.830 U ml^{-1}) in 100 mM Tris buffer, pH 7.7, containing 20 mM $CaCl_2$. Aliquots were taken from the reaction mixture to monitor trypsin activity by a fluorogenic assay (*vide infra*). Batch experiments with the isolated negative feedback loops were performed under the same conditions as for the full CRN, but no trypsinogen was present in the reaction mixture. For the isolated positive feedback loop, trypsinogen (129 μM) was mixed with a catalytic amount of trypsin.

CSTR experiments. Four glass syringes were loaded with trypsinogen (8 mg ml^{-1}, 338 μM in 4 mM HCl, 36 mM $CaCl_2$), trypsin (27 μg ml^{-1}, 1.16 μM in 500 mM Tris-HCl, 20.5 mM $CaCl_2$, pH 7.7), proinhibitor **2** (4.72 mg ml^{-1}, 7.68 mM in 2 mM HCl) and aminopeptidase (ten times the desired final concentration in the CSTR, which varies, in 10 mM Tris-HCl, 10 mM $MgCl_2$, pH 7.7) and connected with tubing to the four inlets of a 250 μl polydimethylsiloxane (PDMS) reactor. Fractions of the total flow rate were 0.5 for trypsinogen (that is, 27.5 μl h^{-1} at a total flow of 55 μl h^{-1}), 0.2 for both trypsin and proinhibitor **2** and 0.1 for aminopeptidase. Aliquots of the reaction mixture were diluted with 150 μl of an aqueous 0.1 M $KHSO_4$ solution to quench all reactions.

Trypsin activity assay. Trypsin activity was measured by mixing 100 µl of the quenched reaction mixture with 3 ml of 5 µg ml^{-1} bis-(Cbz-L-Arg)-rhodamine fluorogenic substrate in 50 mM Tris-HCl, pH 7.7. The increase in fluorescence intensity (λ_{ex} = 450 nm, λ_{em} = 520 nm) was monitored for 40 s and the initial, linear slope was compared to a calibration curve to find the concentration of active trypsin.

Determination of inhibitor species concentration. A volume of 50 µl of the quenched reaction mixture was filtered to remove all enzymes and the filtrate was mixed with tryptophan as an internal standard. The organic compounds in the filtrate were separated by analytical HPLC and were monitored in time with ultraviolet detection at 265 nm. Appropriate peaks were integrated and a calibration curve was used to determine the concentration of inhibitor species.

Amplification of trypsin signal. In addition to the experimental set-up in Fig. 1c, a small, 63 µl CSTR was placed in series after the main 250 µl CSTR. The latter was fed with trypsinogen, trypsin, aminopeptidase (3.30 U ml^{-1}, concentration in syringe) and proinhibitor **2** at a total flow rate of 55 µl h^{-1}. In addition to the inflow from the first CSTR, chymotrypsinogen (concentration in syringe 935 µM in 4 mM HCl, flow rate 55 µl h^{-1}) was fed into the second reactor. Outflowing droplets from the second reactor were diluted with 150 µl 0.1 M $KHSO_4$ to quench all reactions. Chymotrypsin activity was monitored by a chromogenic assay (λ_{abs} = 410 nm) using the substrate *N*-succinyl-Ala-Ala-Pro-Phe-*p*-nitroanilide (0.30 µM in 50 mM Tris, pH 7.7). The increase in absorbance was measured for 60 s. The initial slope was linear and was compared to a calibration curve to determine chymotrypsin activity.

Modulation of trypsin signal. In addition to the experimental set-up in Fig. 1c, a small, unstirred 35 µl reactor was placed in series after the main 250 µl CSTR. The latter was fed with trypsinogen, trypsin, aminopeptidase (3.30 U ml^{-1}, concentration in syringe) and proinhibitor **2** at a total flow rate of 55 µl h^{-1}. One additional inlet was inserted into the second reactor through which both STI (concentration in syringe 7.7 µM in 0.1 M Tris pH 7.7, flow rate 27.5 µl h^{-1}) and the fluorogenic substrate bis-(Cbz-L-Arg)-Rhodamine (concentration in syringe 10.1 µM in 0.1 M Tris pH 7.7, flow rate 160 µl h^{-1}) were supplied. The outlet tubing of the second reactor was imaged from below by fluorescence microscopy (λ_{ex} = 488 nm, λ_{em} = 520 nm) to probe the conversion of the fluorogenic substrate.

Control over complex coacervation. A 250 µl CSTR was fed with trypsinogen, trypsin, aminopeptidase (3.30 U ml^{-1}, concentration in syringe) and proinhibitor **2** at a total flow rate of 55 µl h^{-1}. From every second fraction collected from the outflow of the CSTR, 5 µl was added to a batch reactor containing 25 µl of a complex coacervate solution (final concentrations of 6.25 mM polycation (Ac-(Lys-Ser)$_6$-Lys-OH), 0.535 mM polyanion (H-Glu(Glu)$_{20\text{-}99}$-OH) and 0.23 µM STI). Samples were vortexed and incubated for 10 min at room temperature before analysis. After analysing the contents of the CSTR for 18 h, the final concentration of STI was increased to 0.47 µM. The presence of coacervates was determined by optical microscopy and turbidity measurements using a NanoDrop spectrophotometer.

Received 13 August 2014; accepted 19 November 2014; published online 12 January 2015

References

1. Bray, D. Protein molecules as computational elements in living cells. *Nature* **376,** 307–312 (1995).
2. Koshland, D. E., Goldbeter, A. & Stock, J. B. Amplification and adaptation in regulatory and sensory systems. *Science* **217,** 220–225 (1982).
3. Kholodenko, B. N. Cell-signalling dynamics in time and space. *Nature Rev. Mol. Cell Biol.* **7,** 165–176 (2006).
4. Ferrell, J. E., Tsai, T. Y. & Yang, C. Q. O. Modeling the cell cycle: why do certain circuits oscillate? *Cell* **144,** 874–885 (2011).
5. Yashin, V. V. & Balazs, A. C. Pattern formation and shape changes in self-oscillating polymer gels. *Science* **314,** 798–801 (2006).
6. Stuart, M. A. C. *et al.* Emerging applications of stimuli-responsive polymer materials. *Nature Mater.* **9,** 101–113 (2011).
7. Debnath, S., Roy, S. & Ulijn, R. V. Peptide nanofibers with dynamic instability through nonequilibrium biocatalytic assembly. *J. Am. Chem. Soc.* **135,** 16789–16792 (2013).
8. Elowitz, M. B. & Leibler, S. A synthetic oscillatory network of transcriptional regulators. *Nature* **403,** 335–338 (2000).
9. Hasty, J., McMillen, D. & Collins, J. J. Engineered gene circuits. *Nature* **420,** 224–230 (2002).
10. Kim, J. & Winfree, E. Synthetic *in vitro* transcriptional oscillators. *Mol. Syst. Biol.* **7,** 465 (2011).
11. Franco, E. *et al.* Timing molecular motion and production with a synthetic transcriptional clock. *Proc. Natl Acad. Sci. USA* **108,** 784–793 (2011).
12. Chirieleison, S. M., Allen, P. B., Simpson, Z. B., Ellington, A. D. & Chen, X. Pattern transformation with DNA circuits. *Nature Chem.* **5,** 1000–1005 (2013).
13. Fujii, T. & Rondelez, Y. Predator–prey molecular ecosystems. *ACS Nano* **7,** 27–34 (2013).
14. Montagne, K., Plasson, R., Sakai, Y., Fujii, T. & Rondelez, Y. Programming an *in vitro* DNA oscillator using a molecular networking strategy. *Mol. Syst. Biol.* **7,** 466 (2011).
15. Epstein, I. R. & Showalter, K. Nonlinear chemical dynamics: oscillations, patterns, and chaos. *J. Phys. Chem.* **100,** 13132–13147 (1996).
16. Horváth, J., Szalai, I. & De Kepper, P. An experimental design method leading to chemical Turing patterns. *Science* **324,** 772–775 (2009).
17. De Kepper, P., Epstein, I. R. & Kustin, K. A. Systematically designed homogeneous oscillating reaction: the arsenite-iodate-chlorite system. *J. Am. Chem. Soc.* **103,** 2133–2134 (1981).
18. Taylor, A. F., Tinsley, M. R., Wang, F., Huang, Z. & Showalter, K. Dynamical quorum sensing and synchronization in large populations of chemical oscillators. *Science* **323,** 614–617 (2009).
19. Yoshida, R., Takahashi, T., Yamaguchi, T. & Ichijo, H. Self-oscillating gel. *J. Am. Chem. Soc.* **118,** 5134–5135 (1996).
20. Boekhoven, J. *et al.* Catalytic control over supramolecular gel formation. *Nature Chem.* **5,** 433–437 (2013).
21. Boekhoven, J. *et al.* Dissipative self-assembly of a molecular gelator by using a chemical fuel. *Angew. Chem. Int. Ed.* **49,** 4825–4828 (2010).
22. Carnall, J. M. A. *et al.* Mechanosensitive self-replication driven by self-organization. *Science* **327,** 1502–1506 (2010).
23. He, X. *et al.* Synthetic homeostatic materials with chemo-mechano-chemical self-regulation. *Nature* **487,** 214–218 (2012).
24. Gerdts, C. J., Sharoyan, D. E. & Ismagilov, R. F. A synthetic reaction network: chemical amplification using nonequilibrium autocatalytic reactions coupled in time. *J. Am. Chem. Soc.* **126,** 6327–6331 (2004).
25. Warren, S. C., Guney-Altay, O. & Grzybowski, B. A. Responsive and nonequilibrium nanomaterials. *J. Phys. Chem. Lett.* **3,** 2103–2111 (2012).
26. Goodwin, B. C. Oscillatory behavior in enzymatic control processes. *Adv. Enzyme Regul.* **3,** 425–438 (1965).
27. Novak, B. & Tyson, J. J. Design principles of biochemical oscillators. *Nature Rev. Mol. Cell Biol.* **9,** 981–991 (2008).
28. Kurin-Csörgei, K., Epstein, I. R. & Orbán, M. Systematic design of chemical oscillators using complexation and precipitation equilibria. *Nature* **433,** 139–142 (2005).
29. Boissonade, J. & De Kepper, P. Transitions from bistability to limit cycle oscillations. Theoretical analysis and experimental evidence in an open chemical system. *J. Phys. Chem.* **84,** 501–506 (1980).
30. Aubel, D. & Fussenegger, M. Watch the clock—engineering biological systems to be on time. *Curr. Opin. Genet. Dev.* **20,** 634–643 (2010).
31. Abita, J-P., Delaage, M. & Lazdunsk, M. Mechanism of activation of trypsinogen—role of 4 *N*-terminal aspartyl residues. *Eur. J. Biochem.* **8,** 314–324 (1969).
32. Seely, J. H. & Benoiton, N. L. Effect of *N*-methylation and chain length on kinetic constants of trypsin substrates epsilon-*N*-methyllysine and homolysine derivatives as substrates. *Can. J. Biochem. Cell B* **48,** 1122–1131 (1970).
33. Barkai, N. & Leibler, S. Robustness in simple biochemical networks. *Nature* **387,** 913–917 (1997).
34. Lucasius, C. B. & Kateman, G. Understanding and using genetic algorithms—Part 1. Concepts, properties and context. *Chemometr. Intell. Lab. Sys.* **19,** 1–33 (1993).
35. Priftis, D. & Tirrell, M. Phase behavior and complex coacervation of aqueous polypeptide solutions. *Soft Matter* **8,** 9396–9405 (2012).

Acknowledgements

The authors thank H. Adams for help with peptide synthesis. This work was supported by the European Research Council (ERC, advanced grant 246812 Intercom, to W.T.S.H.), the Netherlands Organization for Scientific Research (NWO, VICI grant 700.10.44, to W.T.S.H.), a Marie Curie Intra-European Fellowship (grant 300519, to S.N.S.) and funding from the Dutch Ministry of Education, Culture and Science (Gravity programme 024.001.035).

Author contributions

W.T.S.H. supervised the research. S.N.S., A.S.Y.W. and W.T.S.H. planned the project and designed experiments. S.N.S. designed the oscillating network, and synthesized and optimized all compounds. S.N.S., A.S.Y.W., S.G.J.P. and J.G. performed experiments and analysed data. S.N.S., A.S.Y.W. and R.M.M. built and refined the model and wrote the required scripts for analysis. A.S.Y.W., R.M.M., H.W.H.R. and T.F.A.G. performed computational simulations. S.N.S., A.S.Y.W., S.G.J.P., T.F.A.G., and W.T.S.H. wrote the manuscript.

Additional information

Supplementary information is available in the online version of the paper. Reprints and permissions information is available online at www.nature.com/reprints. Correspondence and requests for materials should be addressed to W.T.S.H.

Competing financial interests

The authors declare no competing financial interests.